Green Chemistry

Cite this: *Green Chem.*, 2011, **13**, 3230

www.rsc.org/greenchem

PAPER

A sustainable aqueous route to highly stable suspensions of monodispersed nano ruthenia

Capucine Sassoye,*[a,b,c] Guillaume Muller,[a,b,c] Damien P. Debecker,[a,b,c,d] Alejandro Karelovic,[d] Sophie Cassaignon,[a,b,c] Christian Pizarro,[a,b,c] Patricio Ruiz[d] and Clément Sanchez[a,b,c]

Received 29th June 2011, Accepted 9th August 2011
DOI: 10.1039/c1gc15769h

Highly stable suspensions of monodispersed ruthenia nanoparticles have been prepared *via* a sustainable aqueous oxidative pathway. The nanoparticles (2 nm) have been thoroughly characterized by TEM, XRD, XPS, MS-TGA and thermodiffraction. The addition of hydrogen peroxide in the $RuCl_3$ solution provokes a fast oxidation of Ru(III) ions into Ru(IV). This increases the rate of the hydrolysis/condensation reactions and further promotes the nucleation over the growth of the particles. The very high stability conditions of the colloidal suspension have been studied. This aqueous one-step process, which uses no organic solvent or toxic pollutant additive, is quick and produces calibrated ruthenia nanoparticles in high yields. It presents a green alternative to the preparation and use of ruthenia. As examples, two applications are presented. In the first, RuO_2 coatings have been tested for their electrical capacitance. In the second, RuO_2/TiO_2 catalysts, prepared from the controlled deposition of ruthenia nanoparticles on TiO_2 particles, have been proven to be highly effective for the production of methane from CO_2.

Introduction

Nowadays the need of advanced nanostructured materials is critical. Potential applications of nanomaterials are numerous in wide ranges of practical fields. Among them, electrochemical energy storage/conversion device[1–4] and catalysis[5] have attracted much attention. In particular, ruthenium oxide based nanomaterials are versatile and attractive candidates for various technological applications such as supercapacitors,[6,7] electrodes,[8] or catalysts.[9,10] RuO_2 electrodes demonstrate interesting performances for chlorine electrogeneration,[11] water electrosplitting into hydrogen or oxygen,[12,13] or CO oxidation in sensors.[9,14] As a catalyst, ruthenium and ruthenium oxide have shown high performance in various reactions such as alkane combustion,[15] CO_2 methanation[16] and HCl oxidation.[17,18] Moreover, thanks to its high chemical stability in both acidic and alkaline media, RuO_2 can be used under a large range of conditions.

All properties exhibited by RuO_2 based nanomaterials are strongly dependent on the degree of crystallinity, texture, surface area and degree of hydration of the ruthenium oxide phase. As an example in electrochemistry, RuO_2 mesoporous thin films exhibiting capacitance up to 1000 F g^{-1} at 10 mV s^{-1} were recently prepared from ruthenium peroxo-based sols and amphiphilic block copolymers.[19] The fine tuning of the precursor solution and thermal treatment allowed the combined control of the film thickness, mesoporosity and nanocrystallinity. These characteristics explain the excellent capacitance of the materials. Nanostructured catalysts must present high activity and selectivity and good stability over the cycles. This requires a controlled and homogeneous size of the active particles. Materials with high surface area and good particle dispersion are generally required. In addition, the interactions between the particles and the support must be sufficient to prevent sintering. Fine tuning of the preparation process is therefore crucial.

Several pathways have been used to process RuO_2 nanomaterials with controlled morphologies and increased surface areas. From the first syntheses (using the pyrolysis of ruthenium(III) precursors,[20] or the addition of strong base or water to ruthenium precursors) to the hydrothermal synthesis,[21] highly agglomerated nanoparticles with broad size distribution have been obtained. In order to better control RuO_2 surface reactivity, other synthetic pathways have been proposed, leading to porous RuO_2 aerogels,[14] mesoporous RuO_2@SiO_2 where connected RuO_2 crystallites are trapped within SiO_2 aerogels,[22,23] RuO_2 nanorods,[24] nanotubes[25] and mesoporous powders.[26] Recently,

[a]*UPMC Univ Paris 06, Chimie de la Matière Condensée de Paris, UMR 7574, F-75005, Paris, France*
[b]*CNRS, Chimie de la Matière Condensée de Paris, UMR 7574, F-75005, Paris, France*
[c]*Collège de France, Chimie de la Matière Condensée de Paris, UMR 7574, 11 place Marcelin Berthelot, 75231, Paris cedex 05, France*
[d]*Institute of Condensed Matter and Nanoscience - MOlecules, Solids and reactiviTy (IMCN/MOST), Université catholique de Louvain, Croix du Sud 2/17, 1348, Louvain-La-Neuve, Belgium.*
E-mail: capucine.sassoye@upmc.fr; Fax: +33 1 44 27 15 04; Tel: +33 1 44 27 14 34

1.6 nm dispersed RuO_2 particles have been prepared through a non-green synthetic route (use of toluene, pyridine *etc.*) that requires several steps.[27] RuO_2@SiO_2 nanocomposites with catalytic activity in the oxidation of benzyl alcohol have been prepared with the help of bifunctionnal ligands that act as metallic Ru nanoparticle stabilizers and sol–gel promoters.[28,29] These processes are complicated, need a strictly controlled atmosphere, present several steps with unknown yields, are energy/time consuming and use toxic or pollutant reactants.

Our study deals with the green preparation of highly stable and well defined monodispersed aqueous colloidal suspensions of small ruthenia nanoparticles. The high stability of this suspension (several months without any other additive) allows the further implementation of the nanoparticles in various processes. To demonstrate this, two examples of applications are presented. RuO_2 thin films prepared from the nano ruthenia suspensions were tested for their electrical capacitance. Nanostructured RuO_2/TiO_2 catalysts prepared from the controlled deposition of the ruthenia particles on TiO_2 were used in the production of methane from CO_2.

Results and discussion

The particles are easily prepared from an aqueous solution of $RuCl_3$ (heated from 30 min to one week at 95 °C) to which an excess of hydrogen peroxide solution is added. No addition of alkaline solution is required. The solution turns immediately from dark brown to dark black. After being heated at 95 °C and cooled at room temperature, the suspension remains stable. The particles are so stabilized as colloids that even after 4 h of high centrifugation, only partial recovery of the powder is possible indeed the black supernatant remains black. The yield, estimated from the weight of the recovered powder after centrifugation and calcination at 400 °C, reaches 75% for 2 h of heating.

Transmission electron microscopy (TEM) grids have been prepared right after the addition of hydrogen peroxide, and then after 30 min, 2 h, 6 h and one week of heating. As highlighted on TEM pictures (Fig. 1–2), the ruthenia particles are well separated and monodispersed in size. The average diameter of particles reaches 2.0 ± 0.2 nm. This size is somewhat comparable to the one obtained with hydrothermal methods (from 1.6 to 2.6 nm).[21,30] No drastic evolution in the size of the particles with the heating time has been observed.

Energy dispersive X-ray analyses (EDX) on the non washed grids show a dramatic decrease in the amount of chlorine with the heating of the sol (Cl : Ru ratio from 1.0 with no heating to less than 0.1 with 2 h of heating measured by EDX analysis). XPS spectra on well washed powders coming from 2 h heated suspensions show only 0.5 at.% of chlorine. The yield of recovered powder increases from only 20% at 0 or 30 min to more than 75% after 2 h and 92% after 6 h of heating. The suspension remains stable after up to 5 h of heating. On the contrary, the particles in suspension strongly agglomerate with almost no reversibility past 6 h of heating. The supernatant becomes perfectly clear and transparent. The apparent increase in the centrifugation yield with the duration of synthesis is related to the strong evolution of the aggregation state of the particles, and thus their ability to be easily centrifuged.

Crystalline planes are visible on the high resolution TEM (HR–TEM) images (Fig. 2). For the non heated suspensions, the measured planes (mostly distances of 1.86 Å and 1.97 Å) do not correspond to any identified crystalline phase; the distances do not match with those from crystalline ruthenia nor the precursor $RuCl_3$, meaning that the particles only present a chlorinated pre-ruthenia structure. After 2 h of heating, HR–TEM images show the 200 or 111 planes which correspond to anhydrous crystalline ruthenia (2.25 Å and 2.22 Å). It is noteworthy that this high organization is only seen on HR–TEM images after a certain time of observation under the electron beam. It is reasonable to put forward that a "pre-ruthenia" structure is initially formed, which easily evolves towards well-crystallized RuO_2.

Under a less intense electron beam (Fig. 1), planes are not detected, even after a few minutes of electron exposure, showing low organization in the initial rutile structure, as is well known for hydrous ruthenia. However, the crystallinity is detected through large electron diffraction rings. The radii of the rings are perfectly consistent with the 101, 200, 111 and 210 planes of ruthenia. This crystallinity is optimum for the sample heated 2 h at 95 °C and does not improve with a longer heating time, meaning that the hydrous rutile structure is obtained from 2 h of heating.

Accordingly, the X-ray diffraction (XRD) patterns of the particles heated for 2 h show two slight broad shoulders that are consistent with the 110 and 101 planes around $2\theta = 30°$ and the 211 plane around 54° (Fig. 3a). After 6 h of heating the peaks become more distinguishable, but still remain broad. This broadness is related to the small size of the crystalline domain and to the intrinsic disorder due to hydration. Indeed, ruthenia can accommodate structural water (responsible for protonic conduction and high capacity). This structural water disrupts the 3D rutile structure, destroying part of the connection between the RuO_6 octahedra, inducing disorder, and thus lowering the crystallinity.[31]

Thermogravimetric analysis coupled to mass spectrometry (MS–TGA) was performed under air with the particles obtained from the 2 h heated suspension (Fig. 4). At first continuous and slow weight loss is observed and attributed to the departure of water molecules. Accordingly, thermodiffraction (Fig. 3b) shows an increase in intensity and a narrowing of the rutile diffraction peaks, which is consistent with an increase of the crystallinity; the departure of the water molecules allows a better organization of the rutile structure. When the particles obtained from suspensions heated for 2 h at 95 °C are further heated in air at 300 °C or 450 °C, ruthenia 110 planes are clearly visible in the TEM image (Fig. 5). In parallel, the particles grow and sinter (at 300 °C, mainly 5 nm diameter particles mixed with a few 50×15 nm rods; at 450 °C, elongated 20×50 nm particles).

As mentioned in the previous paragraph, the dark colloidal suspensions (heated from 30 min to 5 h) are stable for up to several months after being cooled at room temperature. Concentration of the sol, up to 10 times is possible under vacuum at 40 °C without any precipitation. TEM images of the concentrated or re-diluted suspension clearly show that the suspension remains colloidal, without any aggregation or growth of the particles (Fig. 7). The measured pH after 2 h of heating is 2 (and then does not evolve for months at room temperature). When the pH of the suspension is increased by

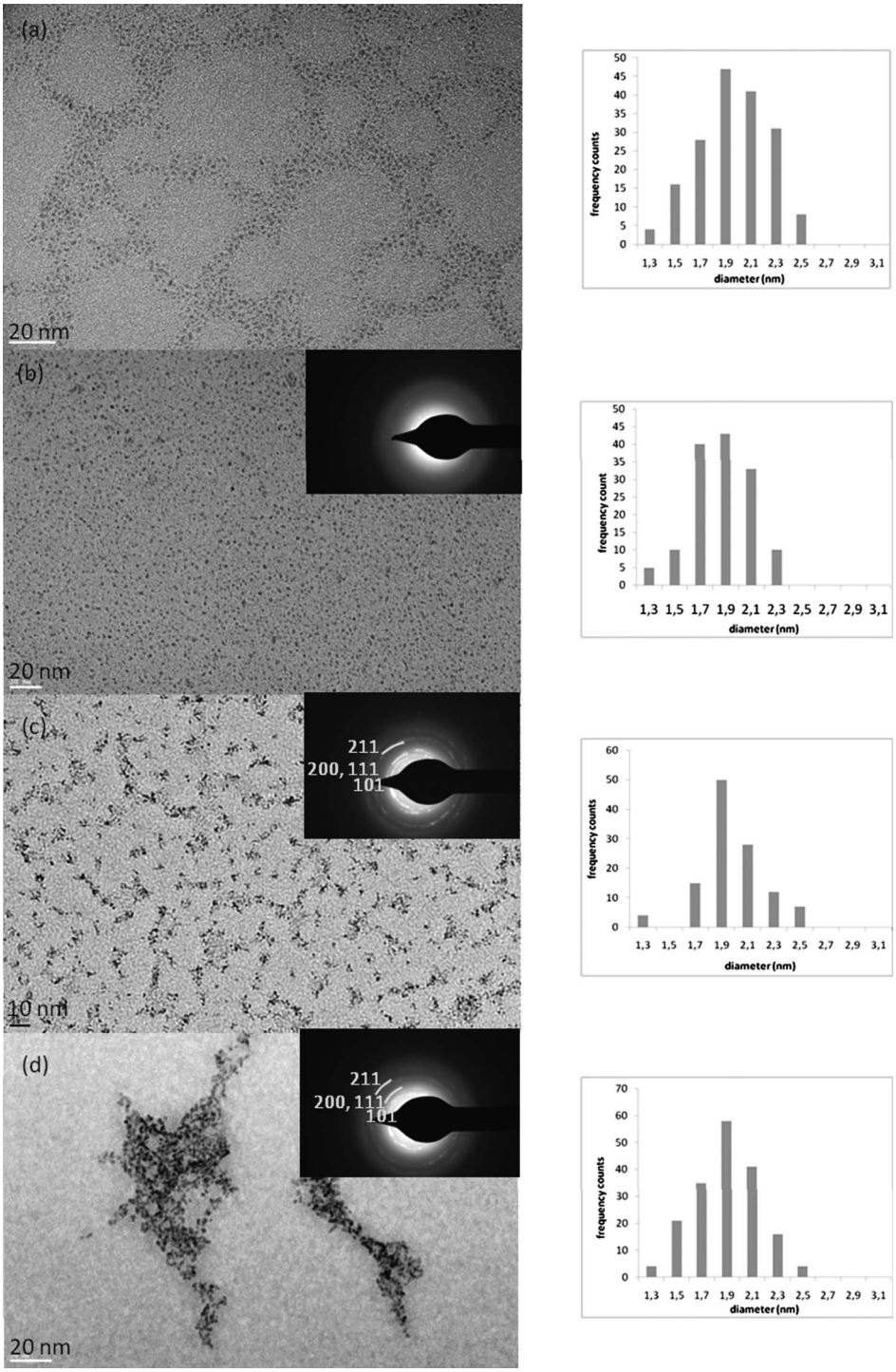

Fig. 1 TEM images, size histograms and selected area electron diffraction (SAED) of as-synthesized $RuO_2 \cdot xH_2O$ particles heated at 95 °C: 0 min (a), 30 min (b); 2 h (c); 6 h (d).

NaOH addition, irreversible RuO_2 agglomeration and then sedimentation start around pH 5 (see Fig. 6). The addition of $AgNO_3$ also leads to agglomeration, conjointly with AgCl precipitation. Cl^- anions in the suspension seem to play a role in the stability of the colloids. As silver chloride precipitates, it is clear that at least some of the Cl^- anions are not trapped in the rutile structure. In view of further applications, this excess of chlorine will advantageously be removed.

The isoelectic point (IEP) has been estimated directly from a 2 h heated suspension. The intersection of the different titration curves at the same point (pH 5) shows that the IEP is close to 5. This value is in accordance with the ones established on hydrous and anhydrous ruthenia.[32] During calcinations, it has been shown that this value can increase to 6 (at 500 °C).

Hydrogen peroxide has the ability to form complexes with most of the transition metal ions.[33] It has been particularly

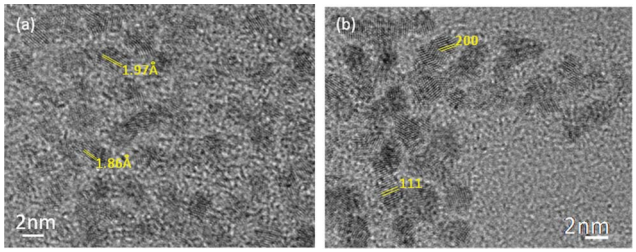

Fig. 2 High resolution TEM pictures of the (a) non heated and (b) 2 h heated solution showing the organization that had occurred under the intense electron beam: ruthenium oxo-chloride precursor of ruthenia from the non heated solution (a) and rutile structure for the particles from the 2 h heated solution (b).

well documented and studied for the titanium case.[34,35] More than the ability to use the titanium(IV) peroxo complexes for analytical application, peroxo ligands are widely used in order to stabilize precursors. In the case of Ru, there is little literature concerning the use of hydrogen peroxide. Few complexes have been reported and always involve other organic ligands.[36,37] In the literature, whenever hydrogen peroxide use is mentioned for the synthesis of ruthenia, only gel[38] or highly agglomerated particles[39] are obtained. In aqueous medium, most reported syntheses of ruthenia involve the addition of a large amount of basic solution, that leads to the precipitation of a black powder. The oxidation of the precursor Ru(III) into Ru(IV) is never questioned and it is assumed to take place during crystallization. In our case, the large excess of hydrogen peroxide allows an immediate oxidation of the ruthenium precursor. It seems to allow fast hydrolysis/condensation rates. Since Ru(IV) is not stable in aqueous solution, this fast nucleation leads to highly dispersed hydrous ruthenia nanoparticles without any growth of the particles. Performing the synthesis in the absence of hydrogen peroxide (with all other parameters being the same) only leads to a black solution. A longer heating of the solution (3 days) is then needed to recover ruthenia which appears to be irreversibly and highly agglomerated. Hydrogen peroxide is thus critical to obtain highly dispersed nanoparticles.

Electrochemical properties of the particles

Ruthenia is well known for its pseudo-capacitive behavior. This behavior is related to the ability of ruthenia to conduct both

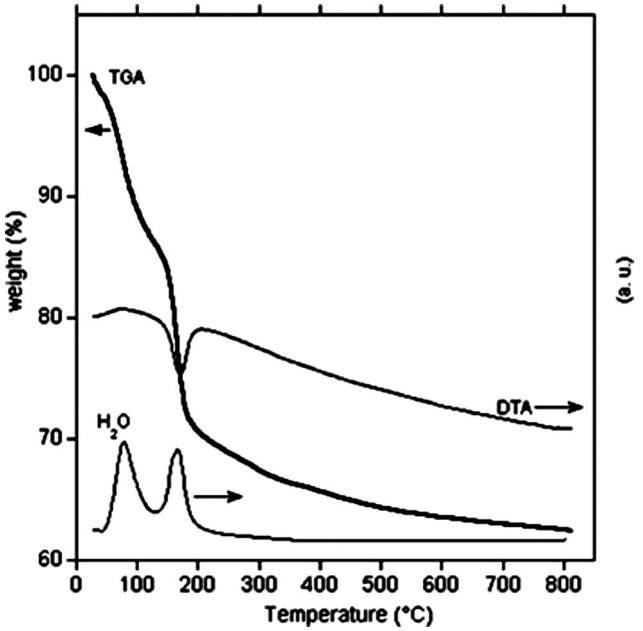

Fig. 4 Thermogravimetric and differential curves of the particles (from 2 h, 95 °C suspensions) associated with the main results of the mass spectroscopy showing the departure of water (5 °C min^{-1}, under air).

electrons and protons. On one hand, the hydrous region (mostly corresponding to the surface) allows facile proton permeation through the material for efficient charge storage. On the other hand, the bulk crystalline anhydrous RuO_2 network accounts for the electronic conduction. High capacitances are the result of the best compromise between both electronic and protonic conduction channels. The charge storage mechanism on RuO_2 based electrodes has been explained by the insertion of electrons and protons at the surface of the material *via* the global equation:[31]

$$Ru^{(IV)}O_a(OH)_b + \delta H^+ + \delta e^- = Ru^{(III)}O_{a-\delta}(OH)_{b+\delta}$$

In order to evaluate the electrical capacity of the produced materials, one drop of ruthenia suspension (2 h, 95 °C) was allowed to dry on a fluorinated tin oxide (FTO) substrate and was further heated for 1 h at 150 °C in air. The measured exposed surface was 0.07 cm^2. Cyclic voltammetry measurements at

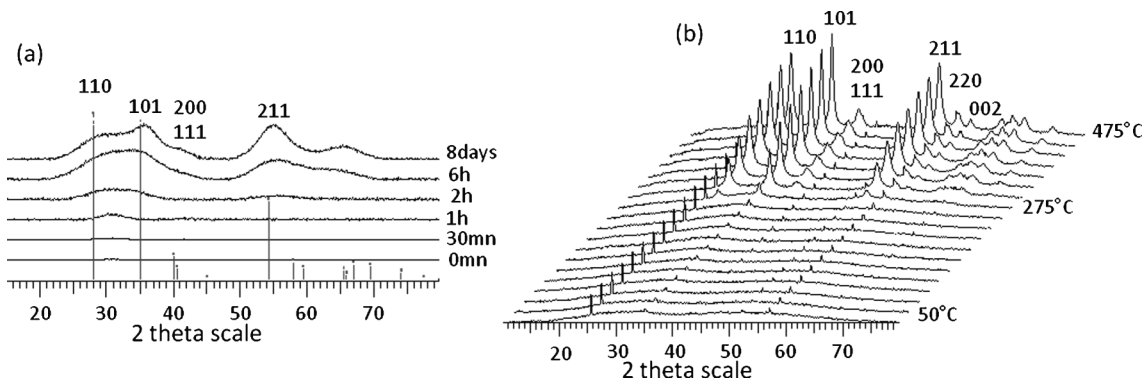

Fig. 3 XRD patterns at room temperature (a) of the as-synthesized nanoparticles heated at 95 °C from 0 min to 8 days, and thermodiffraction patterns; (b) of the 2 h particles from 50 to 475 °C. The main XRD pattern peaks are indexed as the ruthenia structure (ICDD n° 40-1290). * stands for the sample holder.

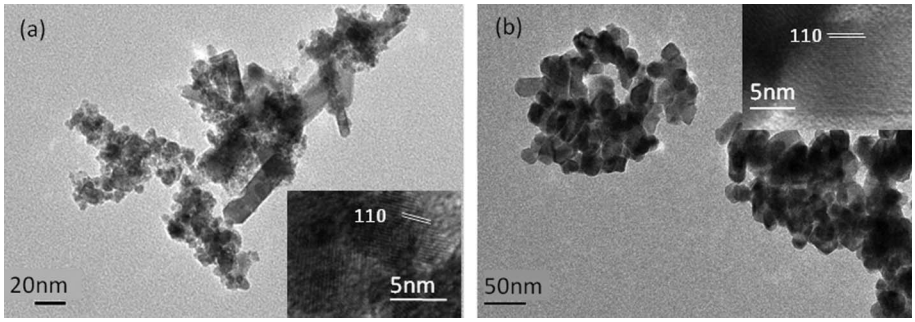

Fig. 5 TEM pictures of the particles heated for 12 h in air at (a) 300 °C and (b) 450 °C.

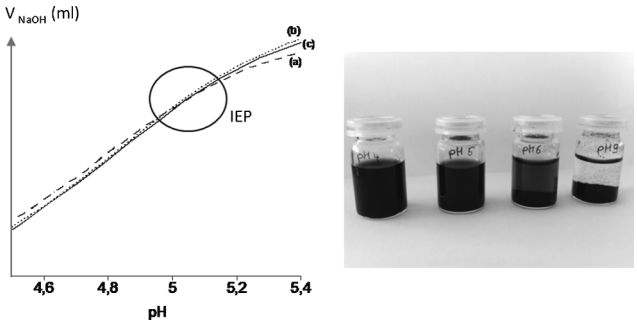

Fig. 6 (left) Volumetric titration of the 2 h heated solution by NaOH 0.02 mol L^{-1} with different $NaNO_3$ concentrations: (a) 0.1, (b) 0.05 and (c) 0.01 mol L^{-1}; (right) stable colloid suspensions after the addition of NaOH until pH 4 and 5, and sedimentation of the particles at pH 6 and 9.

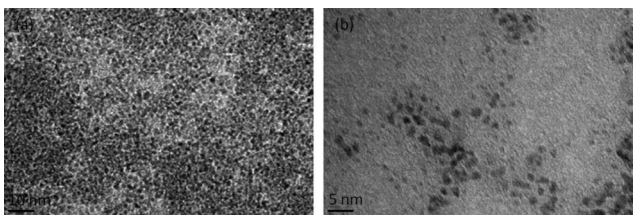

Fig. 7 TEM picture from the 10 times concentrated RuO_2 sol (a), and rediluted RuO_2 sol (b).

different scan rates exhibit a pseudo-capacitance signature (Fig. 8) which is stable over 20 cycles. The rectangular shape of the current density–potential curves (*J*–*E*) reveals the perfect electrochemical reversibility of the redox reactions. This is characteristic of ruthenia; the measured capacity stands at 240 F g^{-1}. The surface capacity reached 33 mF cm^{-2}, which is higher than the latest results on nanotubes[25] or pyridine-capped ruthenia nanoparticles.[27] Thin films can also be processed from an ethanol/water colloidal suspension of RuO_2 particles. Field emission gun scanning electron microscope (FEG–SEM) pictures show that the substrate is entirely covered by RuO_2, with some porosity. These films also present constant pseudo-capacitive behavior over 20 cycles. These results clearly show that the pseudo-capacitance, one of the well known properties of ruthenia, is preserved in the present system. However, the measured values are lower than the best published ones, but one has to keep in mind that the shaping of the films has not been optimized here. Further works will have to consider textural aspects, possible association with other matrices or particles and optimized thermal treatments. The high stability of the ruthenia suspension will most probably promote those further developments.

Catalytic behavior

In connection with current environmental concerns a decisive challenge is to master the catalytic hydrogenation of CO_2 in methane.[40] The development of highly active methanation catalysts is thus an actual field of research.[41–44] In this context, supported Ru-based materials were already identified as

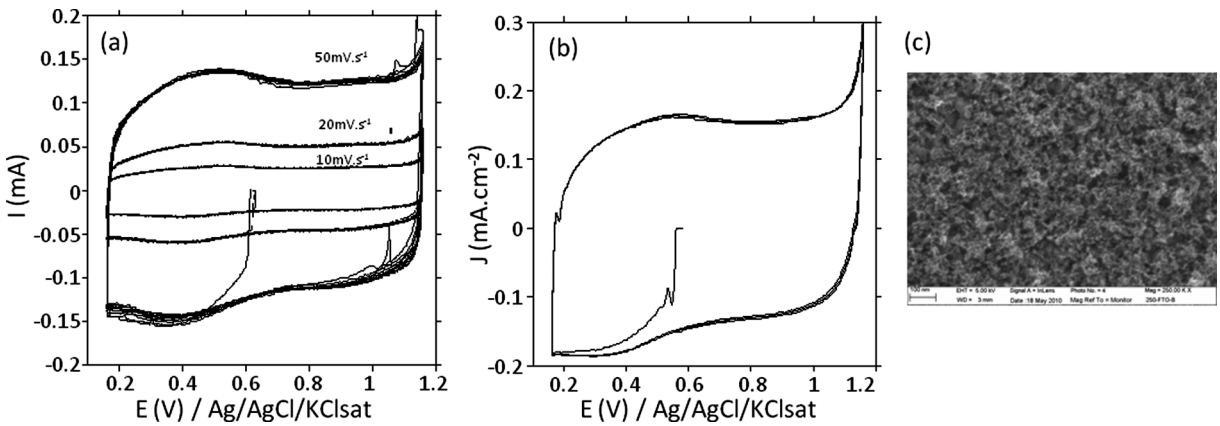

Fig. 8 (a) Cyclic voltammetry of a one drop colloidal suspension deposited on a FTO substrate, heated for 1 h at 150 °C in air; (b) cyclic voltammetry of thin film heated at 200 °C showing a good stability over 20 cycles; (c) FEG-SEM picture of the 200 °C heated film.

promising catalysts and the formation of small nanoparticles was pointed out as a criterion to obtain active and selective catalysts.[16] Catalysts were thus prepared from the as-synthesized RuO_2 nanoparticle suspensions *via* deposition on a commercial TiO_2 powder (Degussa P25; 80% anatase, 20% rutile) classically used as catalyst support.[45] The deposition is followed by calcination in air at 450 °C, to yield a RuO_2/TiO_2 catalyst.

Ruthenia nanoparticles were quantitatively transferred onto the TiO_2 particles. The supernatant was transparent and the final Ru loading in the dried powder was equal to the nominal one (2.2 wt%), as verified by ICP-AES. The 2 nm-sized RuO_2 nanoparticles are distinguished on the surface of the TiO_2 particles (Fig. 9a). Even if the contrast between TiO_2 and RuO_2 is low, it is clear that sintering appears negligible even after calcination at 450 °C (Fig. 9b).

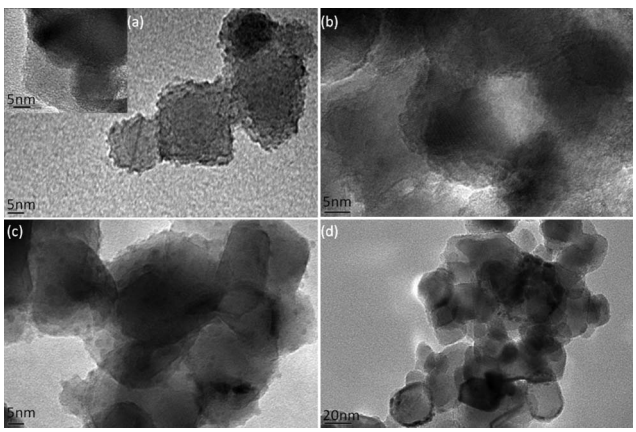

Fig. 9 TEM pictures of TiO_2/RuO_2 powders under different conditions: heated 16 h in air at (a) 150 °C and (b) 450 °C. The 450 °C sample were treated under hydrogen for (c) 2 h at 200 °C and (d) 1 h at 350 °C and tested for catalysis. The inset in (a) represents TiO_2 before RuO_2 adsoption.

Before reaction, the catalyst is reduced *in situ* under H_2. After a 2 h treatment at 200 °C, ruthenium nanoparticles are clearly visible on TEM images (Fig. 9c–d), and on the surface of the TiO_2 particles (Fig. 9c). At 200 °C, this nano-Ru/TiO_2 catalyst exhibits a specific activity of 1.2×10^{-2} mol_{CH4} mol_{Ru}^{-1} s^{-1} (Table 1). This corresponds to a CO_2 conversion of 38%. At this relatively low operation temperature, the selectivity (moles of methane formed/moles of CO_2 reacted) is 100%. No other compounds containing carbon was formed. The superior activity of the nano-Ru/TiO_2 catalyst over a reference sample (WI-Ru/TiO_2, Table 1) prepared by conventional wet impregnation (WI) is clearly demonstrated. The activity of the new nanostructed catalyst is 3-fold as compared to the reference (0.42×10^{-2} mol_{CH4} mol_{Ru}^{-1} s^{-1}). It can be noted that catalytic performance in the same order were obtained with other Ru/TiO_2 catalysts prepared by a sputtering method.[16] The experimental conditions (activation, reaction temperature and contact time) were however not strictly comparable.

When the reduction is carried out at 350 °C for 1 h, the ruthenium particles sinter, form a heterogeneous layer on the surface of the TiO_2 particles (Fig. 9d) and exhibit a lower specific activity of 0.7×10^{-2} mol_{CH4} mol_{Ru}^{-1} s^{-1} (Fig. 9c). This confirms that small nanoparticles are the actual active species.

Table 1 Catalytic methanation of CO_2. Feed: 20 mL min^{-1} composed of CO_2 (10 vol.%), H_2 (40 vol.%) diluted in He at 200 °C

Sample	Metal loading (wt%)	Reduction conditions	Activity (10^{-2} mol_{CH4} mol_{Ru}^{-1} s^{-1})
Nano-Ru/TiO_2	2.2	200 °C, 2 h	1.17
		350 °C, 1 h	0.70
WI-Ru/TiO_2	2.0	200 °C, 2 h	0.42
WI-Rh/TiO_2	2.0	200 °C, 2 h	1.09
WI-Rh/TiO_2	2.0	350 °C, 1 h	0.83

A reference Rh/TiO_2 catalyst (a well-recognized methanation catalyst[42,46]) was prepared by WI and tested under the same conditions. Its activity was similar to the activity reached by our nano-Ru/TiO_2 catalyst. In both cases selectivity is 100%. Bearing in mind that Ru is much cheaper than Rh and considering that the method presented here is not more complicated than the WI method, we believe this new preparation route presents indisputable competitive advantages.

Conclusion

A highly stable suspension of monodispersed ruthenia nanoparticles has been prepared *via* a sustainable aqueous oxidative pathway. The addition of hydrogen peroxide to the ruthenium precursor is directly responsible for the fast oxidation of the Ru(III) species. Hydrogen peroxide seems to increase the speed of the hydrolysis/condensation reactions and promotes nucleation over the growth of the particles. The as-synthesized particles, of which diameters reach 2 nm, present low crystallinity, mainly explained by the small particle size and the intrinsic disorder due to structural water. This combination of partial crystallinity and hydration is desired for electrochemical properties: thin films prepared from ethanolic aqueous RuO_2 suspensions have shown pseudo-capacitive behavior. Dehydration and further calcination of the particles lead to anhydrous highly crystalline ruthenia powder with increased particle size. In order to obtain effective catalysts, a composite of ruthenia and titania has been prepared. As expected, the interaction of these particles on a titanium oxide surface is strong enough to prevent sintering during calcination. The prepared titania-supported ruthenium catalysts have proven to be highly effective for the production of methane from CO_2 with 100% selectivity. Beyond the two examples of applications presented here, the high stability (several months) of this suspension without any other additive opens the door for multiple further uses.

Experimental section

All chemicals were available commercially and used without further purification.

Nanoparticle preparation

A dark brown solution was made from 0.1308 g (0.63 mmol) of $RuCl_3$ dissolved in 40 mL of water. After one minute of stirring, a diluted solution of hydrogen peroxide (3 mL of 30% aqueous H_2O_2 in 20 mL of H_2O) was added dropwise. The pH of the suspension was measured after 5 min of stirring and had dropped from 2.4 to 2.1. The solution was then put

in an oven at 95 °C, for a duration of 30 min to one week without stirring. After cooling, a black colloidal suspension is obtained after up to 5 h of heating. At room temperature, this suspension is stable for several months without further stirring or additives. After 6 h of heating, black powder was recovered from the bottom of a transparent solution. To verify the influence of temperature, immediately after the addition of hydrogen peroxide, a suspension was centrifuged after 10 min of stirring, without heating.

Thin film preparation

One drop (7.2 µL) of the ruthenia particle suspension (2 h, 95 °C) was allowed to dry on a FTO substrate and was further heated for 1 h at 150 °C in air, in order to allow quantification of the RuO_2. The measured exposed surface was 0.07 cm^2.

The black suspension was concentrated to obtain a 0.08 mol L^{-1} concentration. An equal volume of anhydrous ethanol was then added, with 0.061 g of Pluronic F127 $(HO(C_2H_4O)_{106}(C_3H_6O)_{70}(C_2H_4O)_{106}H)$. The solution was cast by dip-coating onto FTO or silicon wafers at a controlled temperature (80 °C) and controlled withdrawal speed (2 mm s^{-1}). The as-synthesized brown films were immediately heated under air at different temperatures (from 120 °C to 300 °C) for 30 min. TEM grids from the concentrated water colloid solution and from the ethanol/water solution showed that the particles were still well separated.

Catalyst preparation

For the nano-Ru/TiO_2 catalyst, an entire batch of previously prepared (2 h, 95 °C) and cooled RuO_2 colloidal suspension was added to TiO_2 P25 (4 g) from Degussa. The mixture was stirred magnetically and heated for 16 h at 50 °C. Water was then evaporated at 50 °C under vacuum (50 mbar). The black powder was then calcined for 16 h at 450 °C under air and washed scrupulously 3 times in water.

The WI-Rh/TiO_2 and the WI-Ru/TiO_2 catalysts were prepared by the wet impregnation of TiO_2 P25 with an aqueous solution of $RhCl_3$ or $RuCl_3$ for 18 h. Water was then evaporated under reduced pressure. The catalysts were then dried and calcined in air at 450 °C for 16 h.

RuO_2 catalytic test

Catalytic tests were carried out using a quartz reactor (U-shaped) with a 0.4 cm internal diameter. A section in the center of the tube is expanded to a diameter of 1 cm, in which catalyst (200 mg) (200–315 µm particle size) was placed and supported by a quartz frit. A thermocouple was in contact with the central part of the catalyst bed and was used to measure and control the temperature. The reaction was carried out at atmospheric pressure, after activation in a 30 mL min^{-1} H_2 flow during 2 h at 200 °C or 1 h at 350 °C (10 °C min^{-1}). Afterwards, the reactor was cooled to 50 °C and the reaction mixture was admitted (20 mL min^{-1} composed of CO_2 (10 vol%), H_2 (40 vol%) diluted in He). The reactor was heated stepwise to 50, 100, 150 and 200 °C, holding 1 h at each temperature. Gas effluent concentrations were determined using a gas chromatograph. All transfer lines were maintained at 120 °C to avoid water condensation.

Transmission Electronic Microscopy (TEM) images were acquired with a FEI Tecnai 120 Twin microscope operating at 120 kV and equipped with a Gatan Orius CCD numeric camera to assess the dispersion, size and crystallinity of the RuO_2 nanoparticles. Samples were prepared by evaporating a drop of aqueous diluted suspensions of the Ru particles on a carbon coated copper grid.

High Resolution Transmission Electronic Microscopy (HR–REM) images were taken on a JEOL 2010 operating at 200 keV, equipped with a Gatan camera.

FEG-SEM images were taken from a field emission gun scanning electron microscope (FEG–SEM Hitachi S4200) performed on a broken piece of coated FTO substrate.

X-Ray Diffraction (XRD) measurements (10–80°) were performed using Cu Kα radiation in a Bruker D8 Advance diffractometer equipped with a Lynx eye detector.

Temperature XRD measurements experiments were recorded on a Panalytical X'PertPro diffractometer equipped with an Anton Paar HTK1200N furnace.

Thermogravimetric analyses (TGA) were performed on a Netzsch STA 409 PC thermobalance coupled with a QMS403C analyzer for mass spectrometry. Solids were heated in an alumina crucible with a heating rate of 5 °C min^{-1} up to 800 °C under air.

Electrochemical properties

The RuO_2 thin films, or the deposited RuO_2 drops were mounted in a three-electrode cell. In the case of the films, part of the working electrode was masked so that an area of 28.3 mm^2 was in contact with the electrolyte solution. A Pt wire was used as the counter electrode while $Ag|AgCl|KCl_{sat}$ was used as the reference electrode ($E°$ = 0.197 V *vs.* SHE, –25 °C). The electrolyte was H_2SO_4 (1 mol L^{-1} in water). Solutions were de-aerated by argon bubbling for 5 min prior to experiments. The cyclic voltammetry experiments were conducted with a potentiostat galvanostat, Princeton Applied Research, 263A, with a scan rate from 10 mV s^{-1} to 50 mV s^{-1}. All the CV curves represent J–E; J being the current density (I divided by the geometric surface of the electrode). Capacitance values were calculated from the voltammetric profiles and normalized to $RuO_2 \cdot xH_2O$ content for the drops, to the exposed surface for the films.

Iso electric point (IEP). The IEP was determined by potentiometric titrations of stable ruthenia suspensions, as obtained after 2 h of heating at 95 °C, meaning that chloride ions are present. The ionic strength was adjusted by addition of $NaNO_3$. The sols were titrated with NaOH (0.02 mol L^{-1}) using Metrohm tritrando 808 potentiograph.

Inductively coupled plasma-atomic emission spectroscopy (ICP-AES). Weight percentages of Ru and Ti were measured by ICP-AES on an Iris Advantage apparatus from Jarrell Ash Corporation. The materials were dried at 105 °C prior to measurements.

Acknowledgements

D. P. Debecker thanks the FNRS for his post-doctoral researcher position. A. Karelovic thanks the Comision Nacional de

Investigacion Cientifica y Tecnologica (Chile) for his PhD student position. The two laboratories are partners of the "Inanomat" IUAP network, sustained by the Service public fédéral de programmation politique scientifique (Belgium). Authors from UCL also acknowledge the Cost Action D41.

References

1 M. Armand and J. M. Tarascon, *Nature*, 2008, **451**, 652–657.
2 P. G. Bruce, B. Scrosati and J.-M. Tarascon, *Angew. Chem., Int. Ed.*, 2008, **47**, 2930–2946.
3 A. Seguatni, M. Fakhfakh, M. J. Vauley and N. Jouini, *J. Solid State Chem.*, 2004, **177**, 3402–3410.
4 C. R. Sides and C. R. Martin, *Adv. Mater.*, 2005, **17**, 125–128.
5 A. T. Bell, *Science*, 2003, **299**, 1688–1691.
6 G. Li, Y. Fan, T. Zhang, T. Ge and H. Hou, *J. Coord. Chem.*, 2008, **61**, 540–549.
7 T. R. Jow and J. P. Zheng, *J. Electrochem. Soc.*, 1998, **145**, 49–52.
8 O. Delmer, P. Balaya, L. Kienle and J. Maier, *Adv. Mater.*, 2008, **20**, 501–505.
9 Z.-P. Liu, P. Hu and A. Alavi, *J. Chem. Phys.*, 2001, **114**, 5956–5957.
10 J. P. Popic, M. L. Avramov-Ivic and N. B. Vukovic, *J. Electroanal. Chem.*, 1997, **421**, 105–110.
11 S. Trasatti, *Electrochim. Acta*, 1991, **36**, 225–241.
12 E. R. Koetz and S. Stucki, *J. Appl. Electrochem.*, 1987, **17**, 1190–1197.
13 A. Mills, P. A. Duckmanton and J. Reglinski, *Chem. Commun.*, 2010, **46**, 2397–2398.
14 K. Reuter and M. Scheffler, *Phys. Rev. B: Condens. Matter Mater. Phys.*, 2006, **73**, 045433–045417.
15 J. Okal and M. Zawadzki, *Appl. Catal., B*, 2009, **89**, 22–32.
16 T. Abe, M. Tanizawa, K. Watanabe and A. Taguchi, *Energy Environ. Sci.*, 2009, **2**, 315–321.
17 N. Lopez, J. Gomez-Segura, R. P. Marin and J. Perez-Ramirez, *J. Catal.*, 2008, **255**, 29–39.
18 C. Mondelli, A. P. Amrute, F. Krumeich, T. Schmidt and J. Perez-Ramirez, *ChemCatChem*, **3**, 657–660.
19 C. Sassoye, C. Laberty, H. Le Khanh, S. Cassaignon, C. Boissiere, M. Antonietti and C. Sanchez, *Adv. Funct. Mater.*, 2009, **19**, 1922–1929.
20 G. Lodi, C. De Asmundis and P. F. Rossi, *Mater. Chem.*, 1977, **2**, 103–108.
21 K.-H. Chang and C.-C. Hu, *Electrochem. Solid-State Lett.*, 2004, **7**, A466–A469.
22 J. V. Ryan, A. D. Berry, M. L. Anderson, J. W. Long, R. M. Stroud, V. M. Cepak, V. M. Browning, D. R. Rolison and C. I. Merzbacher, *Nature*, 2000, **406**, 169–172.
23 K. E. Swider, C. I. Merzbacher, P. L. Hagans and D. R. Rolison, *J. Non-Cryst. Solids*, 1998, **225**, 348–352.
24 D. Susanti, D.-S. Tsai, Y.-S. Huang, A. Korotcov and W.-H. Chung, *J. Phys. Chem. C*, 2007, **111**, 9530–9537.
25 C.-C. Hu, K.-H. Chang, M.-C. Lin and Y.-T. Wu, *Nano Lett.*, 2006, **6**, 2690–2695.
26 S. H. Oh and L. F. Nazar, *J. Mater. Chem.*, 2010, **20**, 3834–3839.
27 Y. Lin, N. Zhao, W. Nie and X. Ji, *J. Phys. Chem. C*, 2008, **112**, 16219–16224.
28 M. Tristany, K. Philippot, Y. Guari, V. Colliere, P. Lecante and B. Chaudret, *J. Mater. Chem.*, 2010, **20**, 9523–9530.
29 V. Matsura, Y. Guari, C. Reye, R. J. P. Corriu, M. Tristany, S. Jansat, K. Philippot, A. Maisonnat and B. Chaudret, *Adv. Funct. Mater.*, 2009, **19**, 3781–3787.
30 K.-H. Chang, C.-C. Hu and C.-Y. Chou, *Chem. Mater.*, 2007, **19**, 2112–2119.
31 D. A. McKeown, P. L. Hagans, L. P. L. Carette, A. E. Russell, K. E. Swider and D. R. Rolison, *J. Phys. Chem. B*, 1999, **103**, 4825–4832.
32 S. Ardizzone, A. Daghetti, L. Franceschi and S. Trasatti, *Colloids Surf.*, 1989, **35**, 85–96.
33 D. Bayot and M. Devillers, *Coord. Chem. Rev.*, 2006, **250**, 2610–2626.
34 G. Schwarzenbach, J. Muehlebach and K. Mueller, *Inorg. Chem.*, 1970, **9**, 2381–2390.
35 J. Lu, L. P. Bauermann, P. Gerstel, U. Heinrichs, P. Kopold, J. Bill and F. Aldinger, *Mater. Chem. Phys.*, 2009, **115**, 142–146.
36 M. M. T. Khan, M. A. Moiz and A. Hussain, *J. Coord. Chem.*, 1991, **23**, 245–256.
37 M. M. T. Khan, A. Hussain, K. Venkatasubramanian, G. Ramachandraiah and V. Oomen, *J. Mol. Catal.*, 1988, **44**, 117–127.
38 J. Pagnaer, D. Nelis, D. Mondelaers, G. Vanhoyland, J. D'Haen, M. K. Van Bael, H. Van den Rul, J. Mullens and L. C. Van Poucke, *J. Eur. Ceram. Soc.*, 2004, **24**, 919–923.
39 K.-H. Chang and C.-C. Hu, *J. Electrochem. Soc.*, 2004, **151**, A958–A964.
40 S. K. Hoekman, A. Broch, C. Robbins and R. Purcell, *Int. J. Greenhouse Gas Control*, 2010, **4**, 44–50.
41 S. Sharma, Z. Hu, P. Zhang, E. W. McFarland and H. Metiu, *J. Catal.*, 2011, **278**, 297–309.
42 S. Eckle, H.-G. Anfang and R. J. Behm, *Appl. Catal., A*, 2011, **391**, 325–333.
43 V. Jimenez, P. Sanchez, P. Panagiotopoulou, J. L. Valverde and A. Romero, *Appl. Catal., A*, 2010, **390**, 35–44.
44 M. Jacquemin, A. Beuls and P. Ruiz, *Catal. Today*, 2010, **157**, 462–466.
45 D. P. Debecker, C. Faure, M.-E. Meyre, A. Derre and E. M. Gaigneaux, *Small*, 2008, **4**, 1806–1812.
46 A. Beuls, C. Swalus, M. Jacquemin, G. Heyen, A. Karelovic and P. Ruiz, *Appl. Catal., B*, 2011, DOI: 10.1016/j.apcatb.2011.02.033.